American Mineralogist, Volume 70, pages 537–548, 1985

High resolution aluminum-27 and silicon-29 nuclear magnetic resonance spectroscopic study of layer silicates, including clay minerals

ROBERT A. KINSEY

School of Chemical Sciences, 505 South Mathews Avenue
University of Illinois at Urbana-Champaign, Urbana, Illinois 61801

R. JAMES KIRKPATRICK, JOHN HOWER[1]

Department of Geology, 1301 West Green Street
University of Illinois at Urbana-Champaign, Urbana, Illinois 61801

KAREN ANN SMITH AND ERIC OLDFIELD

School of Chemical Sciences, 505 South Mathews Avenue
University of Illinois at Urbana-Champaign, Urbana, Illinois 61801

Abstract

High-resolution solid-state magic-angle sample-spinning nuclear magnetic resonance (NMR) spectroscopy of layer silicates, including clay minerals, indicate the following relationships between the NMR parameters and the structures and compositions of the minerals. These relationships are potentially useful in understanding the crystal chemistry of layer silicates and the chemical and structural changes that take place in them during diagenesis and metamorphism. (1) There is a systematic deshielding at silicon (less negative chemical shift) with decreasing Si/(Si + Al(4)). (2) There is a trend of more positive chemical shifts for tetrahedrally-coordinated aluminum with decreasing Si/(Si + Al(4)). (3) There is no systematic relationship between the chemical shift of octahedrally-coordinated aluminum and Si/(Si + Al(4)). (4) There is moderately good agreement between Al(4)/Al(6) ratios determined by NMR and by chemical analysis. (5) The silicon-29 NMR peak breadths of minerals with no Al(4) or with ordered Al(4)/Si arrangements are relatively narrow, while those of most of the other minerals are broader. (6) Paramagnetic impurities (probably iron) in the natural samples cause extensive spinning side-bands which complicate spectral analysis. (7) Higher magnetic field strengths greatly improve spectral resolution for aluminum-27.

Introduction

High-resolution magic-angle sample-spinning (MASS) nuclear magnetic resonance (NMR) spectroscopy of solids is a potentially powerful tool for understanding the structure of materials such as clays and fine grained zeolite catalysts (see e.g., Klinowski et al., 1982). In this paper, we present high-resolution solid-state aluminum-27 and silicon-29 MASS NMR data for a variety of layer silicates, including clay minerals. Our objectives are to determine how the NMR parameters of layer silicates vary with composition and structure, investigating for example, the partitioning of aluminum between tetrahedral and octahedral sites, Si/(Si + Al(4)) ratios, and the extent of Al/Si order in tetrahedral sites.

Our results are in good agreement with the small amount of mostly silicon-29 MASS NMR data that has already been published for layer silicates (Lippmaa et al., 1980, 1981; Barron et al., 1982, 1983; Smith et al., 1983). They are also qualitatively consistent with the relationship between silicon-29 chemical shift and cation–oxygen bond strength developed by Smith et al. (1983).

The results allow, for the first time, the use of solid-state MASS NMR to estimate Si/(Si + Al(4)) ratios, the ratio of tetrahedral to octahedral aluminum, and to some extent the degree of Al/Si order in the tetrahedral layers of sheet silicates of unknown structure.

Methods

NMR spectroscopy

Modern Fourier transform NMR spectroscopy is well described in the book by Farrar and Becker (1971). Applications to solid silicates and aluminosilicates and brief reviews of the theory and methods have been discussed by Lippmaa et al. (1980, 1981), Müller et al. (1981), Smith et al. (1983), and Kirkpatrick et al. (1985).

Spectrometers

Spectra were recorded on three home-built Fourier transform NMR spectrometers (Meadows et al., 1982; Smith et al., 1983).

[1] Deceased.

0003–004X/85/0506–0537$02.00

The first one uses a 3.52 Tesla 4.0-inch bore high-resolution superconducting solenoid (Nalorac Cryogenics, Concord, CA) together with a variety of digital and radiofrequency electronics, including a Nicolet (Madison, WI) model 1280 computer, 293B pulse programmer, and a Control Data Corporation (Oklahoma City, OK) 9427H disc system. The second instrument uses an 8.45 Tesla 3.5-inch bore solenoid (Oxford), a Nicolet 1180 data system with NIC 2090 dual channel transient recorder, and a Diablo (Diablo Systems, Inc., Haywood, CA) model-44B disc system. The third instrument uses an 11.7 Tesla 2.0-inch bore solenoid (Oxford) and a Nicolet 1280/293B data system with Control Data Corporation disc. Both the 8.45 and 11.7 Tesla instruments use Amplifier Research (Souderton, PA) model 200L amplifiers for final rf pulse generation, while the 3.52 Tesla spectrometer is equipped with an Arenburg (Jamaica Plain, MA) model PG 650-C transmitter. All instruments use Andrew-Beams type magic-angle sample-spinning rotor assemblies (Andrew, 1971). At 3.52 Tesla, corresponding to an aluminum-27 resonance frequency of 39.1 MHz, sample volume is about 0.2 ml, and the rotation rates are from about 3 to 5 kHz. At 8.45 Tesla, corresponding to an aluminum-27 resonance frequency of 93.8 MHz and a silicon-29 resonance frequency of 71.5 MHz, sample volume is either 0.2 ml (aluminum-27) or 0.7 ml (silicon-29), and rotation rates are about 3–5 kHz (aluminum) or about 2–3.5 kHz (silicon). At 11.7 Tesla, corresponding to an aluminum resonance frequency of 130.3 MHz or a silicon-29 resonance frequency of 99.3 MHz, sample volume is 0.2 ml, and rotation rates are from about 3 to 5 kHz. The magic angle was set using $^{51}V_2O_5$ or $K^{79}Br$, and for the aluminum-27 spectra was generally offset by 0.5° to eliminate satellite transition background (Oldfield et al., 1982). The 90° pulse widths vary from 1–8 μsec for aluminum and from 20–30 μsec for silicon. Chemical shifts are reported in ppm from external TMS for silicon-29, taken as 6.6 ppm upfield from hexamethyldisiloxane (in $Cr(acac)_3$ doped CH_2Cl_2), and for aluminum-27 are in ppm from the $Al(H_2O)_6^{3+}$ ion in a 1M solution of $Al(H_2O)_6Cl_3$ in water at 20°C. Upfield shifts (increased shielding) are negative for both nuclei, and the estimated errors are ± 0.1 to 1 ppm for silicon depending on the linewidth and resolution, and approximately 1 ppm or greater for aluminum depending on linewidth.

Samples and sample preparation

The samples examined (Table 1) were selected to be representative of both di- and tri-octahedral 2:1 phyllosilicates, although kaolinite and gibbsite were also examined. Major-constituent chemical compositions are available for most samples and are listed in Table 1. The samples include examples with aluminum in octahedral coordination only, tetrahedral coordination only, and in both coordinations. Most natural minerals were from the University of Illinois Mineralogical Collection. Fluorophlogopite is a synthetic material kindly provided by Dr. Hatten S. Yoder of the Carnegie Institute of Washington, Geophysical Laboratory. Synthetic mica-montmorillonite was kindly provided by Professor D. Hendrickson, University of Illinois. Gibbsite ($Al(OH)_3$) was the kind gift of the Alcoa Chemical Corporation (Bauxite, AK). All clay mineral samples (except the smectite, which was run as the bulk bentonite) were particle-size separated into the <1 μm fraction by centrifugal sedimentation to remove non-clay minerals. All samples were examined as finely ground powders (ground with an agate mortar and pestle) in Delrin rotors. No background probe-Al signals (generally due to Al in glass) were visible on any of our spectrometers. All samples were characterized by powder X-ray diffractometry using a Phillips X-ray diffractometer. Electron paramagnetic resonance spectra were obtained at 9 GHz and 23°C for all samples with a Varian (Palo Alto, CA) E-4 spectrometer.

Table 1. Compositions and localities of samples analyzed

		Composition (atoms/10 oxygens)[1]										
Sample	Locality	Al^{VI}	Fe^{+3}	Li^{+1}	Fe^{+2}	Mg	Si	Al^{IV}	K	Na	Ca	X^{+1}
Pyrophyllite[2]	Robbins, NC	2					4					
Gibbsite[2]	Synthetic	2										
Kaolinite[3]	Washington Co., GA	1.97	0.03	----	----	tr	1.99	0.01	tr	tr	tr	
Smectite[3]	Crook Co., WY	1.47	0.18	----	0.02	0.32	3.94	0.06	----	0.20	0.12	
Phlogopite[2]	Franklin, NJ					3	3	1	1			
Fluorophlogopite[2]	Synthetic					3	3	1	1			
Hectorite[4]	Hector, CA	----	----	0.97	----	1.70	3.91	0.09	----	0.27	----	
Talc[2]	Orange Co., NC					3	4					
Muscovite	Methaen Twp., Ont.	1.85	0.11	----	0.01	0.06	3.02	0.98	0.84	0.09	0.01	
Illite	Wind River Canyon, WY	1.66	0.03	----	0.05	0.30	3.43	0.57	0.77	0.01	0.01	
Mica-Montmorillonite[4]	Synthetic	1.99	----	----	----	----	3.37	0.67	----	----	----	0.70
Margarite	Unknown	2					2	2			1	
Illite/Smectites												
A1	Kinnekulle, Sweden	1.55	0.09	----	----	0.41	3.73	0.27	0.43	----	----	0.09
31H	Kinnekulle, Sweden	1.63	0.08	----	----	0.31	3.67	0.33	0.48	----	----	0.11
34H	Kinnekulle, Sweden	1.60	0.10	----	----	0.33	3.79	0.21	0.32	----	----	0.14
39H	Kinnekulle, Sweden	1.44	0.17	----	----	0.43	3.88	0.12	0.22	----	----	0.23

[1] Kaolinite, atoms per 5 oxygens; gibbsite, atoms per 6 oxygens.
[2] Assumed stoichiometric composition.
[3] Analyses from Van Olphen, H. and Fripiat, J. J. (1979) Data Handbook for Clay Minerals and Other Non-Metallic Minerals, Pergamon Press, Oxford.
[4] Analyses from Van Olphen and Fripiat: $CaCO_3$ subtracted from reported analysis of hectorite; gibbsite subtracted from reported analysis of mica-montmorillonite.
[5] Analysis from Robie et al. (1976) J. Res. U.S. Geol. Survey, 4, 631-644.

Magnetic susceptibilities were determined using a CAHN Research (Cerritos, CA) magnetic susceptibility System 6600-1, using the Faraday method.

Results

Silicon-29

We show in Figures 1, 2 and 3 silicon-29 MASS NMR spectra of our samples and summarize in Table 2 the chemical shift results. We observe a range from −76.3 ppm for margarite, to −98.0 ppm for talc, in good agreement with the results of Lippmaa et al. (1980, 1981), who found −98.1 ppm for talc, and −95.0 ppm for pyrophyllite (see also Barron et al., 1983). The kaolinite value of −92.1 ppm and the margarite value of −76.3 ppm agree with the values obtained by Mägi et al. (1981) and Barron et al. (1983). We do not resolve two peaks for our kaolinite, as do Barron et al. for theirs. Our value of −86 ppm for muscovite, which we obtained with several different samples, is slightly different from that of Lippmaa et al. (1980), who reported a poorly split peak with chemical shifts of −84.6 and −86.7 ppm.

Except for the fluorophlogopite, the smaller peaks on either side of the tall peaks are spinning side-bands. These

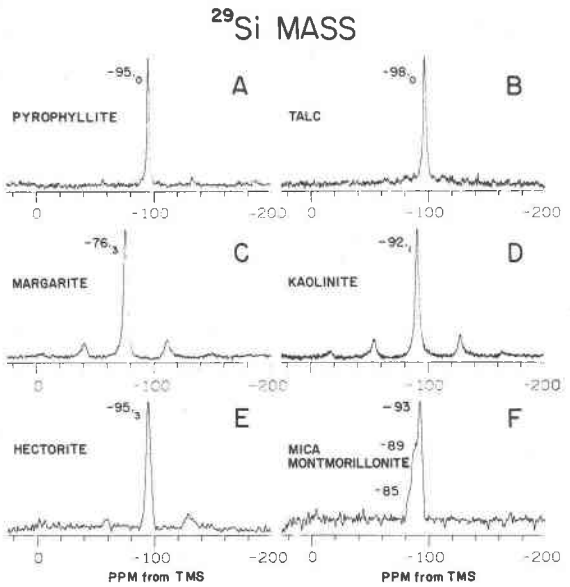

Fig. 1. Silicon-29 MASS NMR spectra of layer silicates at 8.45 and 11.7 Tesla. A, Pyrophyllite (8.45 T), 2.7 kHz MASS, 21 scans at 600 sec recycle time, 30 μsec 90° pulse excitation, 2048 data points, zero-filled to 8192, 25 Hz linebroadening due to exponential multiplication. B, Talc (8.45 T), 1.14 kHz MASS, 17 scans at 300 sec recycle time, 27 μsec 90° pulse excitation, 2048 data points, zero-filled to 8192, 25 Hz linebroadening due to exponential multiplication. C, Margarite (8.45 T), 2.45 kHz MASS, 1325 scans at 10 sec recycle time, 5.3 μsec 53° pulse excitation, 4096 data points, zero-filled to 8192, 25 Hz linebroadening due to exponential multiplication. D, Kaolinite (8.45 T), 2.66 kHz MASS, 3616 scans at 1 sec recycle time, 20 μsec 90° pulse excitation, 2048 data points, zero-filled to 8192, 25 Hz linebroadening due to exponential multiplication. E, Hectorite (8.45 T), 2.44 kHz MASS, 50 scans at 300 sec recycle time, 23 μsec 90° pulse excitation, 2048 data points, zero-filled to 8192, 25 Hz linebroadening due to exponential multiplication. F, Mica-montmorillonite (11.7 T), 4.0 kHz MASS, 2140 scans at 10 sec recycle time, 3.6 μsec 23° pulse excitation, 4096 data points, zero-filled to 8192, 50 Hz linebroadening due to exponential multiplication.

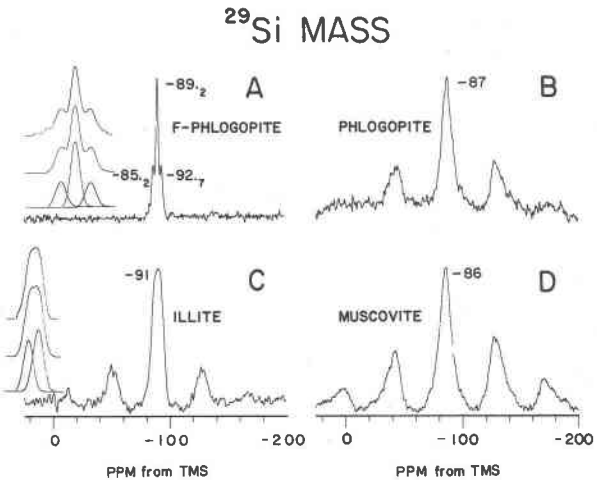

Fig. 2. Silicon-29 MASS NMR spectra of layer silicates at 8.45 and 11.7 Tesla. A, Synthetic fluorophlogopite (11.7 T), 4.0 kHz MASS, 1130 scans at 10 sec recycle time, 3.6 μsec 23° pulse excitation, 4096 data points, zero-filled to 8192, 50 Hz linebroadening due to exponential multiplication. B, Phlogopite (11.7 T), 4.0 kHz MASS, 4471 scans at 10 sec recycle time, 3.6 μsec 90° pulse excitation, 4096 data points, zero-filled to 8192, 50 Hz linebroadening due to exponential multiplication. C, Illite (8.45 T), 2.7 kHz MASS 175 scans at 300 sec recycle time, 16 μsec 90° pulse excitation, 2048 data points, zero-filled to 8192, 50 Hz linebroadening due to exponential multiplication. D, Muscovite (8.45 T), 2.98 kHz MASS, 13005 scans at 168 msec recycle time, 16.1 μsec 90° pulse excitation, 4096 data points, zero-filled to 8192, 50 Hz linebroadening due to exponential multiplication.

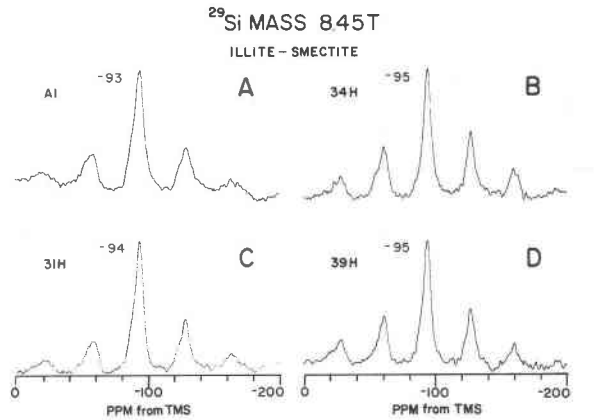

Fig. 3. Silicon-29 MASS NMR spectra of illite-smectites at 8.45 Tesla. The samples were from a mineralogically zoned Swedish bentonite. Spectral conditions all basically as in Fig. 2(C), except the number of scans varies.

Table 2. Siicon-29 (8.45 Tesla) and Aluminum-27 (11.7 Tesla) MASS NMR chemical shifts of samples examined

Sample	Silicon-29 Chemical Shift[a] (ppm)	Tetrahedral Aluminum-27 Chemical Shift[b] (ppm)	Octahedral Aluminum-27 Chemical Shift[b] (ppm)
Pyrophyllite	-95.0	--	4
Gibbsite	--	--	8
Kaolinite	-92.1	--	4
Smectite	N.D.	--	4
Phlogopite	-87	69	--
Fluorophlogopite	-85.2,-89.2,-92.7	69	--
Hectorite	-95.3	66	--
Talc	-98.0	--	--
Muscovite	-86	72	4
Illite	-91	70	4
Mica-Montmorillonite	-83[c],-87[c],-93	70	--
Margarite	-76.3	74	2,-10
Mixed layered Illite-Smectites			
A-1	-93	70	4
31H	-94	69	4
34H	-95	69	4
39H	-95	69	4

[a] In ppm from external Me_4Si.
[b] In ppm from external 1M $Al(H_2O)_6Cl_3$ in H_2O.
[c] Shoulder.

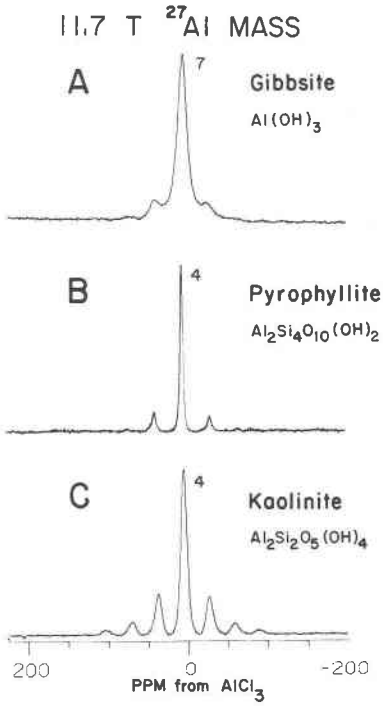

Fig. 4. Aluminum-27 MASS NMR spectra of layer silicates with octahedrally coordinated aluminum, and gibbsite, at 11.7 Tesla. A, Gibbsite, 4.2 kHz MASS, 500 scans at 2 sec recycle time, 3 μsec 90° pulse excitation, 4096 data points, 50 Hz linebroadening due to exponential multiplication. B, Pyrophyllite, 4.5 kHz MASS, 200 scans at 100 msec recycle time, 3 μsec 90° pulse excitation, 8192 data points, 20 Hz linebroadening due to exponential multiplication. C, Kaolinite 4.2 kHz MASS, 1000 scans at 15 sec recycle time, 3 μsec 90° pulse excitation, 4096 data points, zero-filled to 8192, 50 Hz linebroadening due to exponential multiplication.

arise *via* the magic-angle spinning process, and can be distinguished from the true centerband resonances because their positions and intensity vary with spinning speed. The small peaks for fluorophlogopite are all centerband resonances, indicating that nonequivalent silicon sites are present.

Spinning side-bands for silicon-29 may be caused by the presence of a chemical shift anisotropy (CSA) (Smith et al., 1983), by various types of magnetic impurities (most commonly iron either in solid solution or in a separate phase Oldfield et al., 1983), or by dipolar interactions, as interpreted by Grimmer et al. (1983) for an Fe^{2+}-doped olivine. The increase in sideband intensity with magnetic field strength suggests to us that the effect of segregated magnetic domains dominates our samples, although small contributions from substitutional impurities are difficult to rule out. The presence of substitutional paramagnetic impurities is expected to affect isotropic chemical shifts (with a Curie-law dependence), thus, great care is needeed in interpreting small (1–2 ppm) differences in chemical shift for naturally occurring mineral phases. The effect of paramagnetic impurities would be to reduce the shielding (i.e., cause more positive or less negative chemical shifts. The inherent CSA also probably makes a contribution to the side-bands, but in most instances the side-bands are quite prominent and correlate well with the presence of large magnetic susceptibilities. Based on our frequency dependence data, we thus believe that they arise primarily from the presence of small amounts of magnetic impurity domains and that their appearance is unlikely to affect the value of the isotropic chemical shift (Oldfield et al., 1983).

Aluminum-27

We show in Figures 4 through 7 the aluminum-27 MASS NMR spectra of our samples, and summarize in Table 2 the chemical shifts observed. Figure 4 shows the 11.7 T aluminum-27 MASS NMR spectra of gibbsite ($Al(OH)_3$), pyrophyllite ($Al_2Si_4O_{10}(OH)_2$) and kaolinite ($Al_2Si_2O_5(OH)_4$), all of which contain only octahedrally coordinated aluminum (Al(6)). Gibbsite shows a single resonance, consistent with only one type of aluminum site. The chemical shift of 7.8 ppm is consistent with previously reported values for octahedrally coordinated aluminum (Müller et al., 1981; de Jong et al., 1983). Magnetic susceptibility measurements on this sample show it to be diamagnetic, and it exhibits no EPR resonance at 9 GHz and 23°C. The large sidebands are presumably due to Al–Al and AlOH dipole–dipole interactions. Field dependence data (not shown) confirm this.

The aluminum-27 MASS NMR spectra of pyrophyllite and kaolinite also show spectra with significant sideband structure (Fig. 4). These sidebands become less pronounced at lower fields (data not shown) and thus might be attributable to chemical shift anisotropy effects rather than dipole or second-order quadrupole interactions. However, both of these natural mineral samples exhibit modest magnetic sus-

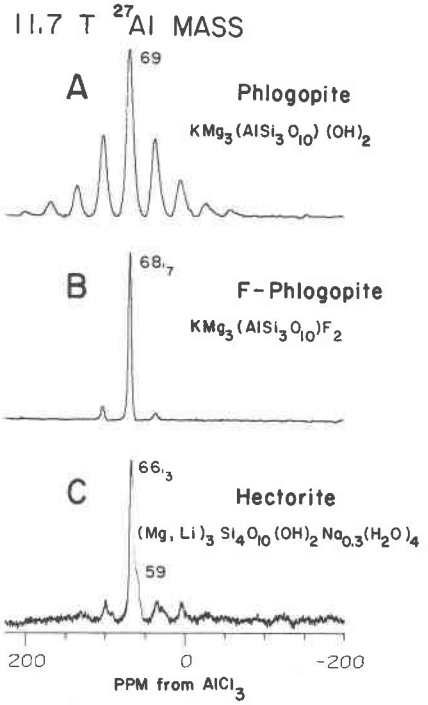

Fig. 5. Aluminum-27 MASS NMR spectra of layer silicates containing tetrahedrally coordinated aluminum, at 11.7 Tesla. A, Phlogopite, 4.1 kHz MASS, 4155 scans at 100 msec recycle time, 3 μsec 90° pulse excitation, 4096 data points, 50 Hz linebroadening due to exponential multiplication. B, Synthetic fluorophlogopite, 4.4 kHz MASS, 600 scans at 30 sec recycle time, 3 μsec 90° pulse excitation, 8192 data points, 25 Hz linebroadening due to exponential multiplication. C, Hectorite, 4.1 kHz MASS, 6400 scans at 100 msec recycle time, 3 μsec 90° pulse excitation, 8192 data points, 25 Hz linebroadenig due to exponential multiplication.

ceptibilities (χ_g of 2.0 and 0.78 × 10^{-6} cgs units for pyrophyllite and kaolinite, respectively), and both have weak EPR absorptions, due at least in the case of kaolinite to Fe^{3+} and lattice defects (Pinnavaia, 1982). As we shall show below, these results, together with the approximate equivalence of the overall aluminum-27 and silicon-29 spectral breadths for pyrophyllite ($\Delta\sigma$ approximately 60 ppm) strongly suggests for both materials a bulk magnetic susceptibility broadening, with concomitant sideband formation upon magic-angle sample-spinning (Oldfield et al., 1983). Nevertheless, the 11.7 Tesla aluminum-27 chemical shift values of 4.0 and 4.4 ppm are consistent with purely octahedral Al coordination in both kaolinite and pyrophyllite.

We show in Figure 5 the 11.7 Tesla aluminum-27 MASS NMR spectra of the minerals phlogopite ($KMg_3AlSi_3O_{10}(OH)_2$) and hectorite (a lithium montmorillonite, $(Mg,Li)_3Si_4O_{10}(OH)_2 \cdot Na_{0.3}(H_2O)_4$ with only a small amount of tetrahedrally coordinated Al) together with the spectrum of synthetic fluorophlogopite ($KMg_3AlSi_3O_{10}F_2$).

The aluminum-27 results for phlogopite indicate Al in exclusively tetrahedral coordination, in accord with the accepted crystal structure for this material, best viewed of as being derived from talc with partial Si → Al(4) substitution, and the presence of charge-balancing interlayer potassium. The chemical shift of 69 ppm from $Al(H_2O)_6^{3+}$ for fluorophlogopite is also consistent with solely tetrahedral aluminum coordination (Fyfe et al., 1982; Müller et al., 1981; de Jong et al., 1983; Kirkpatrick et al., 1985). For hectorite, the peak at 66 ppm is also consistent with tetrahedrally coordinated aluminum, indicating that much of the trace

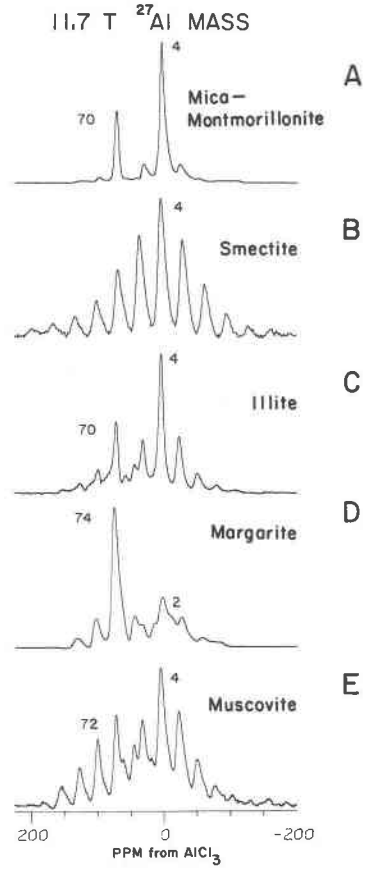

Fig. 6. Aluminum-27 MASS NMR spectra of layer silicates containing mixed aluminum coordination, at 11.7 Tesla. A, Synthetic mica-montmorillonite, 3.4 kHz MASS, 900 scans at 1 sec recycle time, 3 μsec 90° pulse excitation, 4096 data points, 50 Hz linebroadening due to exponential multiplication. B, Smectite, 4.3 kHz MASS, 4000 scans at 100 msec recycle time, 3 μsec 90° pulse excitation, 4096 data points, 100 Hz linebroadening due to exponential multiplication. C, Illite, 3.6 kHz MASS, 3400 scans at 100 msec recycle time, 3 μsec 90° pulse excitation, 4096 data points, 50 Hz linebroadening due to exponential multiplication. D, Margarite, 3.7 kHz MASS, 3900 scans at 100 msec recycle time, 3 μsec 90° pulse excitation, 4096 data points, 50 Hz linebroadening due to exponential multiplication. E, Muscovite, 3.6 kHz MASS, 7000 scans at 100 msec recycle time, 3 μsec 90° pulse excitation, 4096 data points, 50 Hz linebroadening due to exponential multiplication.

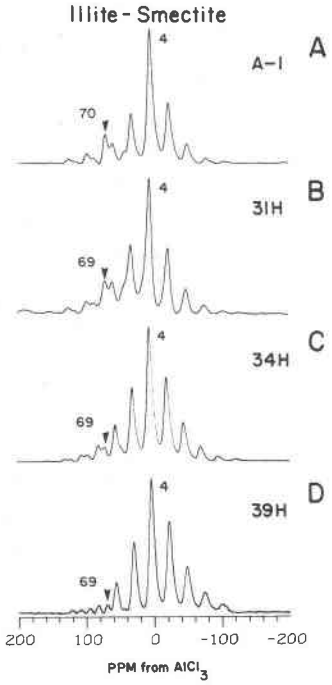

Fig. 7. Aluminum-27 MASS NMR spectra of mixed layer illite-smectites, at 11.7 Tesla. A, A-1, 3.6 kHz MASS, 2000 scans at 100 msec recycle time, 3 μsec 90° pulse excitation, 4096 data points, 50 Hz linebroadening due to exponential multiplication. B, 31H, 3.6 kHz MASS, 2000 scans at 100 msec recycle time, 3 μsec 90° pulse excitation, 4096 data points, 50 Hz linebroadening due to exponential multiplication. C, 34H, 3.3 kHz MASS, 3000 scans at 100 msec recycle time, 3 μsec 90° pulse excitation, 4096 data points, 50 Hz linebroadening due to exponential multiplication. D, 39H, 3.5 kHz MASS, 2000 scans at 100 msec recycle time, 3 μsec 90° pulse excitation, 4096 data points, 50 Hz linebroadening due to exponential multiplication.

aluminum must occupy four-coordinate positions, i.e. that it substitutes for Si rather than (Mg,Li). The shoulder at 59 ppm is probably due to a small amount of feldspar impurity (Kirkpatrick et al., 1985).

A dramatic difference between our results for phlogopite, fluorophlogopite and hectorite is their very large difference in spinning-sideband structure. We believe that such differences originate in the different levels of magnetic impurities found in the natural mineral samples and the synthetic material. We find magnetic susceptibility (χ_g) values of 2.7 $\times 10^{-6}$ cgs units for phlogopite, and 0.67 $\times 10^{-6}$ cgs units for hectorite, together with clear evidence of Fe^{3+} and Mn^{2+} EPR absorptions in phlogopite, and a broad, weak absorption at a g-value of about 2 for hectorite, but no appreciable magnetic susceptibility or EPR absorption for the fluorophlogopite. Thus, there appears to be a good correspondence between the presence of spinning-sideband structure and the presence of magnetic impurities, as we observed for the octahedrally coordinated aluminum (Fig. 4). Moreover, our results indicate a close similarity between the actual magnitudes of the aluminum-27 and silicon-29 magnetic shift anisotropies of both phlogopite and hectorite, consistent with this type of broadening mechanism.

Figure 6 shows the 11.7 T aluminum-27 MASS NMR spectra of phyllosilicates with both octahedral and tetrahedral aluminum. These spectra clearly show both Al(6) resonances, in the range 2.5 to 4.2 ppm, and Al(4) resonances, in the range 70.2 to 74.5 ppm (Müller et al., 1981; de Jong et al., 1983). The smectite does not show a well defined Al(4) resonance because of the low Al(4) concentration. The spinning side-band structures are quite variable. The extremes are the muscovite, with many, and the synthetic mica-montmorillonite, with few. All natural samples do, however, have large magnetic susceptibilities, χ_g, ranging from about 2.0 to 5.6 $\times 10^{-6}$ cgs units. There are also EPR absorptions at 9 GHz and 23°C for muscovite and smectite. These results again suggest a large magnetic susceptibility broadening contribution to the observed sideband structure in the natural minerals.

We show in Figure 7 the 11.7 T aluminum-27 MASS NMR spectra of four mixed-layered illite-smectites from a mineralogically zoned Swedish bentonite. The proportion of illite in these illite-smectites ranges from 65% in A-1 to 40% in 39H. There is a concomitant change in composition, including the amount of Al(6), as indicated by structural formula calculations (Table 1). All spectra show a large peak due to octahedral aluminum, and a smaller peak of varying relative intensity due to tetrahedral aluminum. Once again, the sidebands arise from magnetic impurities, as judged from χ_g values and EPR spectra (data not shown).

In order to obtain the most accurate Al(4)/Al(6) coordinate ratios, it is necessary to understand the origins of all spectral features observed, and to answer the question—what magnetic field strength is best for such determinations? We shall now consider this matter briefly.

For quadrupolar nuclei, the most likely source of linebroadening is the second-order quadrupole interaction (Nolle, 1977; Meadows et al., 1982; Müller et al., 1981), which decreases with increasing magnetic field strength and with sample spinning although to only about 1/4 to 1/10 of the breadth of the spectrum of the static sample. The second most likely sources of static linebroadening are dipolar and chemical shift anisotropy broadening, with average to zero under very fast magic-angle rotation. In addition, as we discussed above, bulk susceptibility (and also potentially dipolar) broadening and sideband formation may also contribute for natural minerals having magnetic impurities. This effect increases linearly with increasing field strength when magnetic domains are present (Oldfield et al., 1983). These points are illustrated by the sets of aluminum-27 MASS NMR data taken at 11.7 and 3.52 Tesla shown in Figure 8. These spectra show decreased peak widths at high field (decreased residual second order breadth), but more intense spinning sidebands, due to a large susceptibility broadening. In addition, the chemical shifts are observed to be field dependent due to a second order quadrupolar shift, with the effect being largest for

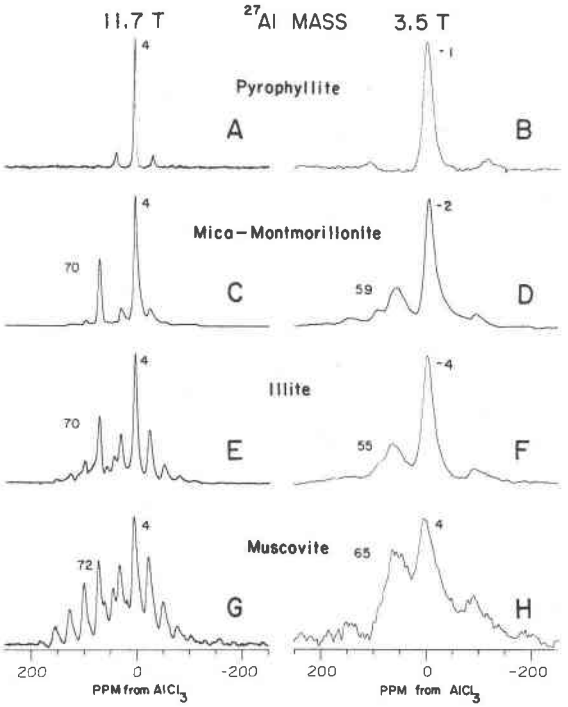

Fig. 8. Aluminum-27 MASS NMR spectra of layer silicates at 3.5 and 11.7 Tesla. A, Pyrophyllite, (11.7 T), 4.5 kHz MASS, 500 scans at 2 sec recycle time, 3 μsec 90° pulse excitation, 4096 data points, 50 Hz linebroadening due to exponential multiplication. B, Pyrophyllite (3.5 T), 3.1 kHz MASS, 3600 scans at 250 msec recycle time, 3 μsec 90° pulse excitation, 4096 data points, 100 Hz linebroadening due to exponential multiplication. C, Mica-montmorillonite (11.7 T), 3.4 kHz MASS, 900 scans at 1 sec recycle time, 3 μsec 90° pulse excitation, 4096 data points, 50 Hz linebroadening due to exponential multiplication. D, Mica-montmorillonite (3.5 T), 3.9 kHz MASS, 80000 scans at 100 msec recycle time, 3 μsec 90° pulse excitation, 4096 data points, 100 Hz linebroadening due to exponential multiplication. E, Illite (11.7 T), 3.6 kHz MASS, 3400 scans at 100 msec recycle time, 3 μsec 90° pulse excitation, 4096 data points, 50 Hz linebroadening due to exponential multiplication. F, Illite (3.5 T), 3.4 kHz MASS, 10000 scans at 100 msec recycle time, 3 μsec 90° pulse excitation, 4096 data points, 100 Hz linebroadening due to exponential multiplication. G, Muscovite (11.7 T), 3.6 kHz MASS, 7000 scans at 100 msec recycle time, 3 μsec 90° pulse excitation, 4096 data points, 100 Hz linebroadening due to exponential multiplication. H, Muscovite (3.5 T), 3.9 kHz MASS, 10100 scans at 100 msec recycle time, 3 μsec 90° pulse excitation, 4096 data points, 100 Hz linebroadening due to exponential multiplication.

Al(4). The linewidths for Al(4) also seem to decrease most on increasing field strength.

These results are all consistent with the dominance of a second-order quadrupolar linebroadening mechanism at low field (3.52 T), and a magnetic susceptibility anisotropy one at high field (11.7 T). Resolution due to the decrease in the second order broadening increases at H_0^2, while the decrease in resolution due to magnetic impurities increases as H_0. For our materials, the overall effect is an increase in resolution with increasing field strength, albeit with the production of more intense spinning sidebands.

The results in Figure 8 also indicate a slight difference in the response of Al(4) and Al(6). The apparent chemical shifts of both Al(4) and Al(6) increase with increasing field-strength, due to the decrease of the second-order frequency shift (Abragam, 1961), but the effect is about twice as large for Al(4) as for Al(6). This difference in behavior, together with the increase in relative peak height (decreased breadth) for the Al(4) resonances indicates a larger nuclear quadrupole coupling constant for the tetrahedral sites. Comparion with data obtained at 8.45 Tesla (data not shown) indicates that the 11.7 Tesla chemical shifts are very close to the unperturbed values.

The results in Figure 8 clearly indicate that optimum resolution of Al(4) from Al(6) is obtained at the highest magnetic field strengths possible—even in samples containing magnetic impurities. The number of lines is greater but they are narrower. Notably, however, even at high field considerable care needs to be taken to choose a spinning speed and spinning angle that yields optimum resolution. Figure 9 compares a static aluminum-27 NMR spectrum of illite-smectite A-1, a spectrum taken exactly "on angle", and a spectrum "off angle" by 0.5°. Optimum resolution is obtained 0.5° off angle, which reduces the number of satel-

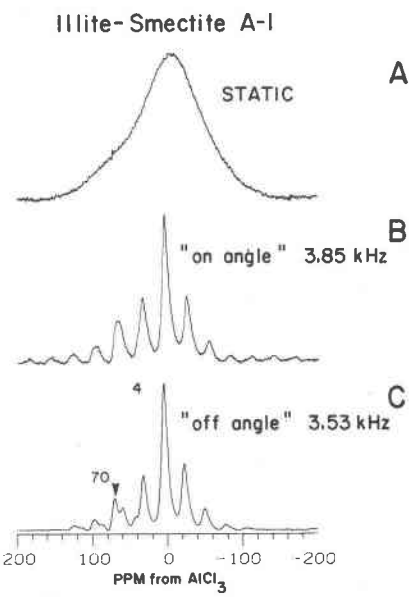

Fig. 9. Static, MASS "on angle", and MASS "off angle" aluminum-27 NMR spectra of Illite-Smectite A-1, at 11.7 Tesla. A, Static, 6000 scans at 100 msec recycle time, 3 μsec 90° pulse excitation, 4096 data points, 50 Hz linebroadening due to exponential multiplication. B, MASS "on angle", 3.85 kHz MASS, 2000 scans at 100 msec recycle time, 3 μsec 90° pulse excitation, 4096 data points, 50 Hz linebroadening due to exponential multiplication. C, MASS "off angle", 3.53 kHz MASS, 6000 scans at 100 msec recycle time, 3 μsec 90° pulse excitation, 4096 data points, 50 Hz linebroadening due to exponential multiplication.

lite side-bands, and at a spinning speed which puts the Al(4) peak *between* the side-bands of the large Al(6) resonance. Spinning slightly off angle broadens the side-bands of the satellite transitions, eliminating them from the spectrum, as discussed by Oldfield et al. (1983).

Discussion

The major objectives in this work are to determine how the aluminum-27 and silicon-29 chemical shifts and silicon-29 peak breadths of well characterized layer silicates vary with structure and composition, and to begin to use these results to understand the structures and crystal chemistries of unknown materials. Our results to date indicate that MASS NMR can be used to examine the following crystal chemical features of layer silicates: Al/Si ratio in the tetrahedral sites, Al/Si ordering in the tetrahedral sites, and the partitioning of aluminum between tetrahedral and octahedral sites.

Tetrahedral Al and Si: chemical shifts

The Al/Si ratio in the tetrahedral sites appears to affect both the silicon-29 chemical shift and that of aluminum-27 in tetrahedral sites. Figure 10A shows the relationship between the silicon-29 chemical shift and Si/(Si + Al(4)) ratio obtained from chemical analysis, or the stoichiometric formula if the material has not been analyzed. The data for kaolinite are not included because it does not have the 2 :1 structure of the other materials. The results in Figure 10A show a clear decrease in the shielding at the silicon nulceus

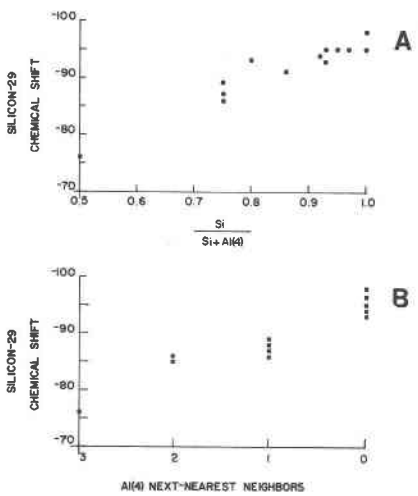

Fig. 10. Correlation between silicon-29 chemical shift and crystal chemical structure. A, Plot of silicon-29 MASS NMR chemical shifts versus Si/(Si + Al(4)), a measure of the composition of the tetrahedral layer. For fluorophlogopite and mica-montmorillonite only the largest peak is plotted. B, Plot of silicon-29 MASS NMR chemical shifts versus (interpreted) number of next-nearest-neighbor tetrahedrally-coordinated aluminums. For fluorophlogopite and mica-montmorillonite all three peaks or shoulders are plotted. For illite, the two shifts from a spectral simulation are plotted.

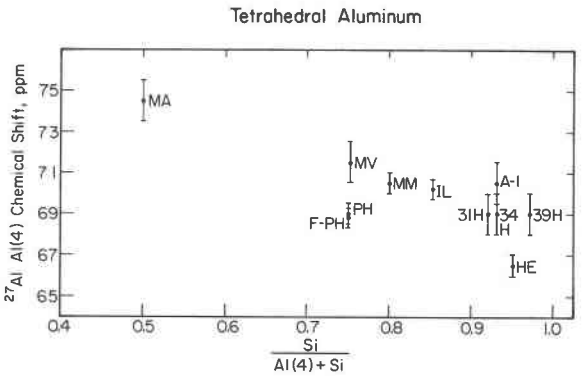

Fig. 11. Plot of 11.7 Tesla aluminum-27 MASS NMR chemical shifts of tetrahedral aluminum versus Si/(Si + Al(4)), a measure of the composition of the tetrahedral layer.

(less negative chemical shift) with increasing Al(4). The octahedral cation appears to have little systematic effect, because although pyrophyllite and talc are 3 ppm apart, muscovite and phlogopite have nearly the same chemical shift. Much of the scatter is probably due to inaccuracies in the chemical analyses.

The trend of Figure 10A is qualitatively consistent with the model of Smith et al. (1983) that relates increased shielding (increasingly negative silicon-29 chemical shifts) to increasing values of the sum of the cation-oxygen bond strengths of the four oxygen atoms surrounding the silicon. It is also similar to the deshielding effect observed with increasing aluminum content in framework silicates (Lippmaa et al., 1981). Unfortunately, accurate structure refinements are not available for most of these materials, so the cation–oxygen bond strength sums cannot be calculated. As with the framework silicates, however, increasing tetrahedral aluminum content leads to decreasing bond-strength sums and, therefore, to less negative silicon-29 chemical shifts.

The Si/(Si + Al(4)) ratios also appear to be correlated with the chemical shift of aluminum(4). Results are plotted in Figure 11. Note that the aluminum-27 chemical shifts of the trioctahedral layer silicates apparently fall about 3 ppm below the trend for the dioctahedral layer silicates. Although a tentative conclusion, it appears that Al in the octahedral sites causes a larger deshielding at Al(4) than does Mg. It also again appears that aluminum in tetrahedral coordination causes an overall deshielding effect—this time at Al(4) itself. The relationship in Figure 11 should be used with care, however, because chemical shifts were obtained at a magnetic field strength of 11.7 Tesla and will be lower (less positive) at lower field strengths. In addition, if the margarite point is eliminated, and the error bars increased by 1 ppm, the correlation weakens considerably.

Finally, our results show that there is no systematic relationship between the aluminum-27 chemical shift of octahedrally coordinated aluminum and the Si/(Si + Al(4)) ratio. Although octahedral aluminum in margarite is slight-

ly more shielded, the chemical shifts of octahedral aluminum in the other materials are indistinguishable.

Tetrahedral Al and Si: order and disorder

One question about layer silicates that has been difficult to answer using diffraction methods is the extent of Al/Si ordering in the tetrahedral sites. This question can be addressed using silicon-29 NMR, because the presence of multiple peaks, and to some extent of increased peak breadths, indicate a range of shieldings at the silicon nucleus, and therefore a range of chemical and structural environments. Because of poorer spectral resolution, such questions are more difficult to answer with the quadrupolar nuclei, such as aluminum-27.

Such relationships are well understood in feldspars. For ordered low albite and microcline the three crystallographically-distinct silicon sites appear as narrow, resolved peaks with full-widths at half-height (FWHH) of about 1 ppm. These sites have either one or two aluminum next-nearest neighbors (Lippmaa et al., 1980; Smith et al., 1983; Kirkpatrick et al., 1985). In disordered high-temperature sanidine, however, the resonances are broadened into one peak with two poorly defined maxima, having a FWHH of about 10 ppm. Similar phenomena due to Si/Al disordering seem to occur in the layer silicates.

The narrowest silicon-29 peaks are for the layer silicates with no tetrahedral aluminum (talc, pyrophyllite, and kaolinite). For these samples the FWHH's are 2 to 4 ppm. The slightly increased breadth of these resonances over those of the feldspars may be due to broadening from magnetic impurities. For margarite, which has Si/(Si + Al(4)) of about 0.5, the FWHH is almost as small (4 ppm), and there is only one peak, which seems to imply that margarite contains an ordered arrangement of aluminum and silicon in the tetrahedral sites. Thus, each silicon has three aluminum next-nearest neighbors and no silicon next-nearest neighbors (a Q^3(3Al) site in the nomenclature of Lippmaa et al., 1981). Because Si/(Si + Al(4)) is 0.5 for margarite, this arrangement implies that no tetrahedral aluminum has a tetrahedral aluminum next-nearest neighbor, and that the aluminum avoidance principle, which states that aluminum atoms avoid each other as next-nearest neighbors (Loewenstein, 1954), is obeyed. Farmer and Velde (1973) have previously provided evidence of tetrahedral ordering in margarite on the basis of sharp infrared spectra and the lack of Al–O–Al vibrations, and Guggenheim and Bailey (1975) have refined a margarite in the space group Cc, indicating full ordering. However, Guggenheim and Bailey (1975) also found that for their sample of margarite the two tetrahedral sheets within the 2 :1 layer were not compositionally identical, having Al(4) contents of 1.006 and 0.877. If this were true of our sample, the silicon-29 spectrum would have an additional peak attributable to Q^3(2Al) silicon sites, which it does not. To ensure that we are not missing a peak with a very long relaxation time (T_1) we ran a silicon-29 spectrum of margarite assuming a T_1 of 4000 seconds. The spectrum is identical to that in Figure 1C.

For muscovite and phlogopites, the silicon-29 NMR data suggest that there is more than one silicon site present and, therefore, that Al/Si ordering in the tetrahedral layers is not perfect. Extremely strong evidence of this is the spectrum of synthetic fluorophlogopite (Fig. 2A). The spectrum consists of a central peak at −90.2 ppm and smaller, but equal sized peaks at −85.2 and −92.7 ppm. These resonances are not spinning side-bands, because they are not disposed at the spinning frequency and do not shift position with spinning speed. Because phlogopite has Si/(Si + Al(4)) = 0.75, in a perfectly ordered sample all silicons would have one aluminum next-nearest neighbor (Q^3(1Al)). We interpret the large peak at −89.2 ppm as due to these Q^3(1Al) sites, and by analogy with the previously observed deshielding effect of Al(4) in zeolites and feldspars, the small peak at −92.1 ppm as due to Q^3(0Al) sites, and the small peak at −85.2 ppm as due to Q^3(2Al) sites. The small peaks are equal in height, because their abundance must be the same in order to maintain an average Q^3(1Al) composition. The presence of Q^3(0Al) and Q^3(2Al) sites in this sample is very strong evidence for a lack of perfect Al/Si ordering in the tetrahedral sites. From the simulation of the spectrum in Figure 2A, it appears that about 46% of the silicon sites are not Q^3(1Al). The spectrum of fluorophlogopite is very well resolved (FWHH about 2 ppm) due to its lack of magnetic impurities.

The silicon-29 MASS NMR spectra of the natural phlogopite and muscovite (Figs. 2B and 2D) are also consistent with some Al/Si disorder, although because the large peak breadths observed could arise entirely from broadening due to magnetic impurities, it is impossible to be more definite than this.

The spectrum of the synthetic mica montmorillonite (Fig. 1F) also shows signals from three silicon sites. This sample has Si/(Si + Al(4)) between 1.00 and 0.75 so the "average" silicon site should be between Q^3(0Al) and Q^3(1Al), and the material must contain both types of sites. We interpret the largest peak, at −93 ppm, to be from Q^3(0Al) sites, the shoulder at −87 ppm to be from Q^3(1Al) sites, and the small shoulder at −83 to be from Q^3(2Al) sites. In this spectrum the presence of the Q^3(2Al) sites, which are not required by stoichiometry, indicates significant Al/Si disorder in the tetrahedral layers. (Again, we assume no macroscopic heterogeneity.)

The silicon-29 MASS NMR spectra of the Swedish illite-smectites (Fig. 3) are also consistent with the presence of multiple silicon sites, and potentially Al/Si disorder on the tetrahedral sites. These clays have Si/(Si + Al(4)) between 0.97 and 0.92 and, consequently, should have mostly Q^3(0Al) silicon sites and some Q^3(1Al) sites.

We have attempted to simulate each of the illite-smectite spectra shown in Figure 3. Many combinations of peak height and breadth gave reasonable fits, but all successful simulations contain a large peak at about −93 to −96 ppm (Q^3(0Al)), and smaller peaks at about −87 ppm (Q^3(1Al)) and at −83 ppm (Q^3(2Al)). The Q^3(1Al) peak was always larger than the Q^3(2Al) peak. These results again suggest the presence of Al/Si disorder in the tetrahedral sites.

The silicon-29 MASS NMR spectrum of hectorite, and its simulation, indicate mostly $Q^3(0Al)$ and a small number of $Q^3(1Al)$ silicon sites. The material has Si/(Si + Al(4)) of about 0.95, requiring almost all $Q^3(0Al)$ sites, in agreement with the NMR data.

Because a number of the phases we have examined contain more than one type of silicon site, we have replotted the silicon-29 chemical shifts versus number of next-nearest neighbor aluminums in the tetrahedral layers (Fig. 10B). This plot contains the three sites in the synthetic fluorophlogopite and mica-montmorillonite and the two sites in illite (Fig. 2C). The correlation is excellent, and is similar to that of Lippmaa et al. (1981) for tectosilicates. This presentation of the data also explains why the mica-montmorillonite falls off the trend of the plot of silicon-29 chemical shift versus Si/(Si + Al(4)) (Fig. 10A). That is, the largest peak, which is the one plotted in Figure 10A, corresponds to a $Q^3(0Al)$ site and not to the bulk composition.

Al(4)/Al(6) ratios

Another important structural parameter for layer silicates is the Al(4)/Al(6). Until now, this ratio, like Si/(Si + Al(4)), could only be determined by chemical analysis and allocation of the components into the available sites by calculating idealized structural formulae.

Using spectral simulations and integrations of the aluminum-27 MASS NMR spectra, however, it is now possible to determine the relative amounts of tetrahedral and octahedral aluminum. Spectra obtained at 11.7 T (or above) should give the best results, because they have the best resolution. Our simulations were done using the Nicolet curve fitting routine, CAP. This program allows for input of up to 28 separate lines of varying intensity, width, and position. Lorentzian, Gaussian, or Voight linebroadening functions are available. The program is interactive, and gives an rms % error as a measure of the goodness-of-fit of the simulation.

The spectra of fluorophlogopite, pyrophyllite, kaolinite, and phlogopite, all of which have only one aluminum site, were simulated to help determine typical variations in the amount of Lorentzian or Gaussian character of the lines. Figure 12 shows a typical aluminum-27 MASS NMR spectrum for illite smectite A-1, together with its simulation. The simulation uses a 100% Lorentzian linebroadening and has an rms error of 4.3%. The largest discrepancy between simulation and experiment appears to be that the experimental lines are not exactly symmetrical, generally being skewed to the low ppm side, due presumably to a small residual second order broadening effect. The simulation in Figure 12 yields an Al(4)/Al(6) ratio of 6.2, in good agreement with the value of 5.7 determined by chemical analysis.

Similar simulations have been carried out for all the samples that contain both tetrahedral and octahedral aluminum. Table 3 lists the samples studied and the Al(4)/Al(6) ratios determined by chemical analysis and by NMR. The NMR determined numbers are the average values obtained from simulations of experimental spectra

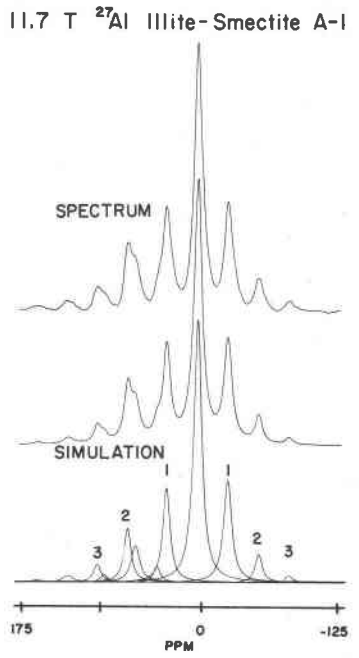

Fig. 12. Aluminum-27 MASS NMR spectra and simulation of illite-smectite A-1. The spectrum was taken with 3.8 kHz MASS, 4000 scans at 100 msec recycle, 4096 data points and 50 Hz linebroadening due to exponential multiplication. The simulation used 100% Lorentzian linebroadening. The numbers indicate the order of spinning-sideband for Al(6).

taken at several spinning speeds, and with different spectral phasings. For most, the results from two or three spinning speeds were averaged.

As may be seen from Table 3, the agreement between the Al(4)/Al(6) ratios determined by chemical analysis and by NMR is rather good. The only samples with significant disagreement are the margarite and the 31H illite-smectite. With these exceptions, the rms errors in the percent Al(4) determined by NMR range from 2 to 4%. The lowest error is for the synthetic mica montmorillonite, which has only a very small spectral overlap between the octahedral and tetrahedral resonances. The highest error is for muscovite,

Table 3. Comparison between Al(4)/Al(6) ratios determined by chemical analysis and by NMR

Sample	Al(4)/Al(6) Chemical Analysis	Al(4)/Al(6) NMR
Muscovite	1.9	1.9
Illite	2.9	2.6
Mica-Montmorillonite	3.0	3.0
Margarite	1.00	0.56
Mixed layered Illite-Smectites		
A-1	5.7	6.7
31H	4.9	7.3
34H	7.6	10.1
39H	12.0	15.7

for which both sideband patterns are very broad (about 100 ppm), and thus overlap considerably. Changing the percent Gaussian character of the peaks does not significantly affect the Al(4)/Al(6) ratios determined. In general, the rms errors range from 3.5 to 9%, with 7% being about average.

The margarite sample offers some puzzling results in addition to the poor agreement between the NMR and chemical composition. Careful selection of spinning speed permits resolution of *two* octahedral lines, one at 4 ppm, the other at −10 ppm. The −10 ppm line and its sidebands account for about 7% of the total aluminum intensity. In the determination of the Al(4)/Al(6) ratios, this intensity was included in the amount of octahedral aluminum. The chemical shift of −10 ppm is unusual, being much more shielded than the octahedral lines for aluminas (R. A. Kinsey, unpublished data) and other sheet silicates.

The relationships between Si/(Si + Al(4)) and silicon-29 and aluminum-27 chemical shifts (Figs. 10 and 11) and the ability to calculate Al(4)/Al(6) ratios offer an opportunity to very rapidly and accurately obtain a great deal of structural and compositional data for layer silicates. Because Si + Al(4) must total four (neglecting Fe^{3+}) in a ten-oxygen formula unit, NMR uniquely defines the composition of that layer.

An important potential application of aluminum-27 NMR spectroscopy of sheet silicates is in the examination of the clay size fraction of shales undergoing burial diagenesis. Hower et al. (1976) have shown that the percent of illite layers and Al_2O_3 in mixed-layer illite-smectites from the U.S. Gulf Coast increase in a complex way with depth. This change in aluminum content and any associated changes in Al(4)/Al(6) partitioning should be detectable by NMR methods.

Finally, we note that, perhaps even more than usual with NMR, considerable care must be exercized in the acquisition and interpretation of aluminum-27 MASS NMR spectra when quantitative results are required. For the materials we have investigated, high field operation yields chemical shifts that are essentially those which would be obtained in the absence of any second-order quadrupole shift—the same cannot be said for results obtained at lower field, e.g., with 200 MHz (^1H equivalent) instruments, which are present in many laboratories. Moreover, we are fortunate that the quadrupole coupling constants in clays appear to be fairly small (about 1–2 MHz), but are not too small. For example, in $Al(H_2O)_6Cl_3$, all three transitions may be excited by an r.f. pulse, causing intensity anomalies (data not shown, see e.g., Schmidt, 1971) while with many other minerals (Ghose and Tsang, 1973), e^2qQ/h values are very large (up to 10 to 15 MHz), resulting in complex sideband patterns for the central transition in a MASS NMR experiment. Clearly, it is necessary to obtain spectra for Al(4)/Al(6) quantitation at several pulse width settings in order to ensure that both sites behave in the same manner. When very complex mixtures containing second phases, especially feldspars and other clays, are investigated, such detailed studies become even more essential. Nevertheless, when such detailed investigations are carried out in combination with silicion-29 MASS NMR, unique insight into the structures of layer silicates, including clay minerals, can be obtained.

Acknowledgments

This paper is dedicated to the memory of Professor John Hower. John was among the first to recognize the usefulness of solid-state MASS NMR spectroscopy in investigating silicate minerals and was instrumental in bringing us all together to work on the problem. We will miss his insight and guidance.

This work was supported in part by the National Science Foundation Grants EAR8207260 and EAR8408421 and the Texaco Corporation, and has benefitted from facilities made available by the University of Illinois—National Science Foundation Regional NMR Instrumentation Facility.

References

Abragam, A. (1961) The Principles of Nuclear Magnetism. Clarendon Press, Oxford.

Andrew, E. R. (1971) The narrowing of NMR spectra of solids by high-speed specimen rotation and the resolution of chemical shift and spin multiplet structures for solids. Progress in NMR Spectroscopy, 8, 1–39.

Barron, P. F., Wilson, M. A., Campbell, A. S., and Frost, R. L. (1982) Detection of imogolite in soils using solid state ^{29}Si NMR. Nature, 299, 616–618.

Barron, P. F., Frost, R. L., Skjenitad, J. O., Koppi, A. J. (1983) Detection of two silicon environments in kaolins by solid state ^{29}Si NMR. Nature, 302, 49–50.

de Jong, B. H. W. S., Schramm, C. M. and Parziale, V. E. (1983) Polymerization of silicate and aluminate tetrahedra in glasses, melts, and aqueous solutions-IV. Aluminum coordination in glasses and aqueous solutions and comments on the aluminum avoidance principle. Geochimica et Cosmochimica Acta, 47, 1223–1236.

Farmer, V. C. and Velde, B. (1973) Effect of structural order and disorder on the infrared spectra of brittle micas. Mineralogical Magazine, 39, 282–288.

Farrar, T. C., and Becker, E. D. (1971) Pulse and Fourier transform NMR: introduction to theory and methods. Academic Press, New York.

Fyfe, C. A., Gobbi, G. C., Klinowski, J., Thomas, J. M., and Ramdas, S. (1982) Resolving crystallographically distinct tetrahedral sites in silicalite and ZSM-5 by solid-state NMR. Nature, 296, 530–536.

Ghose, S., and Tsang, T. (1973) Structural dependence of quadrupole coupling constant e^2qQ/h for ^{27}Al and crystal field parameter D for Fe^{3+} in aluminosilicates. American Mineralogist, 58, 748–755.

Grimmer, A. -R., von Lampe, F., Mägi, M. and Lippmaa, E. (1983) High resolution ^{29}Si NMR of solid silicates: influence of Fe^{2+} in olivines. Zeitschrift für Chemie, 23, 343–344.

Guggenheim, S., and Bailey, S. W. (1975) Refinement of the margarite structure in subgroup symmetry. American Mineralogist, 60, 1023–1029.

Hower, J., Eslinger, E. V., Hower, M. E. and Perry, E. A. (1976) Mechanism of burial metamorphism of argillaceous sediment: 1. mineralogical and chemical evidence. Bulletin of the Geological Society of America, 87, 725–737.

Kirkpatrick, R. J., Kinsey, R. A., Smith, K. A., Henderson, D. M., and Oldfield, E. (1985) High resolution solid state sodium-23, aluminum-27, and silicon-29 nuclear magnetic resonance spec-

troscopic reconnaissance of alkali and plagioclase feldspars. American Mineralogist, 70, 106–123.

Klinowski, J., Ramdas, S., Thomas, J. M., Fyfe, C. A. and Hartman, J. S. (1982) A re-examination of Si, Al ordering in zeolites NaX and NaY. Journal of the Chemical Society, Faraday Transactions II, 78, 1025–1050.

Lippmaa, E., Mägi, M., Samoson, A., Engelhardt, G., and Grimmer, A. -R. (1980) Structural studies of silicates by solid-state high-resolution ^{29}Si NMR. Journal of the American Chemical Society, 102, 4889–4893.

Lippmaa, E., Mägi, M., Samoson, A., Tarmak, M., and Engelhardt, G. (1981) Investigation of the structure of zeolites by solid-state high-resolution ^{29}Si NMR spectroscopy. Journal of the American Chemical Society, 103, 4992–4996.

Loewenstein, W. (1954) The distribution of aluminum in the tetrahedra of silicates and aluminates. American Mineralogist, 39, 92–96.

Mägi, M., Samoson, A., Tarmak, M., Engelhardt, G., and Lippmaa, E. (1981) Studies of the structure of silicates and zeolites by solid-state high-resolution silicon-29 NMR spectroscopy. Doklady Akademii Nauk SSSR, 261, 1169–1174.

Meadows, M. D., Smith, K. A., Kinsey, R. A., Rothgeb, T. M, Skarjune, R. P., and Oldfield, E. (1982) High-resolution solid-state NMR of quadrupolar nuclei. Proceedings of the National Academy of Science of the United States, 79, 1351–1355.

Müller, D., Gessner, W., Behrens, H. J., and Scheler, G. (1981) Determination of the aluminum coordination in aluminum-oxygen compounds by solid-state high-resolution ^{27}Al NMR. Chemical Physics Letters, 79, 59–62.

Nolle, A. (1977) Second-order quadrupole splittings of the ^{95}Mo NMR signal in $Mo(CO)_6$ and their reduction by sample spinning. Zeitschrift für Physik A, 280, 231–234.

Oldfield, E., Kinsey, R. A., Smith, K. A., Nichols, J. A., and Kirkpatrick, R. J. (1983) High-resolution NMR of inorganic solids, influence of magnetic centers on magic-angle sample-spinning lineshapes in some natural aluminosilicates. Journal of Magnetic Resonance, 51, 3215–327.

Pinnavaia, J. (1981) Electron spin resonance studies of clay minerals. Developments in Sedimentology, 34, 139–161.

Robie, R. A., Hemingway, B. S., and Wilson, W. H. (1976) The heat capacities of calorimetry conference copper and of muscovite $KAl_2(AlSi_3)O_{10}(OH)_2$, pyrophyllite $Al_2Si_4O_{10}(OH)_2$, and illite $K_3(Al_7Mg)(Si_{14}Al_2)O_{40}(OH)_8$ between 15 and 375 K and their standard entropies at 298.15 K. Journal of Research of the U. S. Geological Survey, 4, 631–644.

Schmidt, V. H. (1971) Pulse response in the presence of quadrupolar splitting. Proceedings of the Ampere International Summer School II, Yugoslavia, 75–83.

Smith, K. A., Kirkpatrick, R. J., Oldfield, E., and Henderson, D. M. (1983) High-resolution silicon-29 nuclear magnetic resonance spectroscopic study of rock forming silicates. American Mineralogist, 68, 1206–1215.

Manuscript received, December 13, 1983;
accepted for publication, November 19, 1984.